*Article*

# Internal Quantum Efficiency of UV μLED Chips

**Yoshihiko Muramoto \*, Masahiro Kimura \* and Akihiro Kondo \***

NITRIDE SEMICONDUCTORS Co., Ltd., 115-7, Itayajima, Akinokami, Seto-cho, Naruto-shi,
Tokushima 771-0360, Japan

\* Correspondence: muramoto@nitride.co.jp (Y.M.); kimura@nitride.co.jp or nitride@nitride.co.jp (M.K.);
a_kondo@nitride.co.jp (A.K.); Tel.: +81-88-683-7750

check for updates
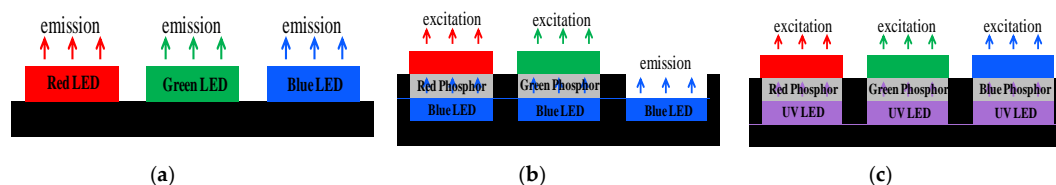
**Abstract:** Micro light emitting diode (μLED) displays have been in development since 2017, aimed for application in 2020. However, when using three-color, i.e., red, blue, and green LEDs, or blue LEDs that excite red and green phosphors, many challenges arise in mass production, cost, and quality. Our group has devised an ultraviolet (UV)-excited red, green, and blue (RGB) display that excites red, green, and blue phosphors using UV-LEDs. This paper studies how the composition and crystal defects of a light-emitting layer affect the luminous efficiency of a UV μLED chip from the perspective of internal quantum efficiency (IQE). It was confirmed that the luminous efficiency improves by making the LED chips in the near ultraviolet range μ-size. The UV μLED chip emitting at 385 nm exhibited a more linear output than a 400-nm purple μLED chip.

**Keywords:** UV-LED; μUV-LED; UV-RGB; μLED; Display

## 1. Introduction

Recently, organic Electro Luminescence (EL) displays are being increasingly adopted in smartphones. This material functions as a self-luminous display, which requires no backlight, and boasts excellent contrast in addition to a wide viewing angle. However, owing to low color reproducibility and concerns regarding durability in high-temperature environments, research and development of micro light emitting diode (μLED) displays is still ongoing [1,2]. In a μLED display, the sub-pixels for colors R (red), G (green), and B (blue) independently emit light, power consumption is low, and the inorganic material is durable over a long lifetime. In particular, μLED displays are deemed useful for applications in wearable devices, in which flexibility and power consumption are important. However, the realization of μLED displays faces many challenges. μLED chips are 10–20 μm$^2$ in size, and a smartphone display requires 2 million pieces of micro LEDs. Moreover, the μLED needs to emit all three colors uniformly with linear control of intensity. Productivity and cost are also important. Display systems with three different LEDs, shown in Figure 1a [3], or a blue LED system in which red and green (RG) phosphors are excited by the blue LED shown in Figure 1b [4] are mainstream. Our group is developing an ultraviolet (UV)-excited RGB system that excites red, green, and blue phosphors using underlying UV-LEDs, as shown in Figure 1c [5].



**Figure 1.** Types of Micro light emitting diode (μLED) displays. (**a**) Three-LED system (**b**) Blue LED + RG phosphor system (**c**) UV-LED + RGB phosphor system.

In the three-LED system, $Al_xIn_yGa_{1-x-y}N$ is grown on a sapphire substrate to form blue and green LEDs, whereas $Al_xIn_yGa_{1-x-y}P$ is generally grown on a GaAs substrate to form the red LED; however, microchips cannot be fabricated in this manner because the materials are fragile. This challenge led to the development of GaN-based red LEDs [6,7]. Although InGaN-based blue LEDs have been reported to achieve external quantum efficiency (EQE) of 80% or more [8], the EQE of InGaN-based green LEDs is still about 30% [9]. Because of droop [10], the green LED exhibits much lower luminous efficiency than the blue LED [11]. Additionally, even if these problems are addressed, synchronous control may be complicated because the band gaps, driving voltages, and reaction speeds are different for the different colors. Furthermore, though the problem of mounting can be avoided by unifying the structure with a blue LED if we adopt an InGaN blue LED + RG phosphor system, this raises difficulties in achieving color balance and synchronization because the blue LED is self-luminous and the red and green LEDs are excited by a blue light; in this case, the light intensities are significantly different and some differences in reaction speeds are also expected. In the UV-LED + RGB phosphor system where each RGB color is realized by exciting phosphors using a UV-LED with a wavelength of 385 nm, the inside of the RGB element is a flip chip with the same AlInGaN material and the same lateral chip-electrode structure, and these features decrease the difficulty of mounting. Furthermore, as the luminescent efficiency of the phosphor material is improved on the side having shorter wavelength, the range of available RGB phosphor materials broadens. UV light from a UV-LED contains some purple but does not greatly affect the excitation light color, and the high color reproducibility due to high excitation efficiency simplifies the achievement of color balance, synchronization, and controllability [12,13]. This article reports tests of the internal quantum efficiency (IQE) to reveal how the material, composition, and structure of UV μLEDs affects performance characteristics in the near-UV region.

## 2. Materials and Methods

Using Metal Organic Chemical Vapor Deposition (MOCVD) originally designed in-house equipment, four wafers for wavelengths of 385 nm and 400 nm were grown on a sapphire substrate and Patterned Sapphire Substrate (PSS) (Figure 2). Although the basic epitaxial structure is the same, the In composition of the InGaN light-emitting layer differs. In addition, super-lattice structures (n-SLS and p-SLS) were included with the 385-nm chip to increase the n-type and p-type carriers. The specification of the sapphire substrate is C-plane 0.2 degree off and the PSS (Figure 3) is 2.0 μm in height (a), 3.75 μm in diameter (b), 4.0 μm in pitch (c), and 0.25 μm in terms of spacing (d).
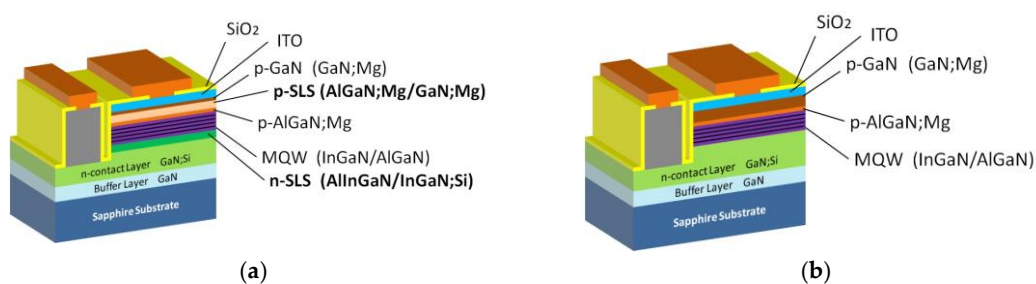


(**a**)        (**b**)

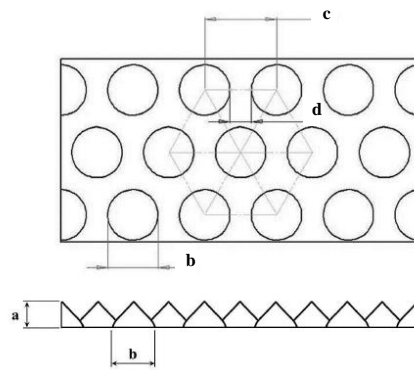**Figure 2.** Epitaxial structure (**a**) 385 nm, (**b**) 400 nm.

**Figure 3.** Patterned Sapphire Substrate (PSS) geometry.

Eight types of chips were fabricated on the four types of wafers to compare changes in characteristics on the basis of size. Figure 4 illustrates the corresponding process steps. The shapes included five types of squares: $24 \times 24$, $48 \times 48$, $72 \times 72$, $144 \times 144$, $288 \times 288$ μm; and three types of rectangles: $12 \times 48$, $24 \times 48$, and $24 \times 72$ μm (Figure 5).

| Process | Top view | Cross view | Detail |
|---|---|---|---|
| ISO | | Isolation etching — MQW + p-GaN, n-GaN, Sapphire | ✓ Etched to Sapphire ✓ Each chip size formation |
| MESA | Light Emitting Area | MESA etching — ITO, MQW + p-Gan, n-GaN, Sapphire | ✓ ITO etching ✓ MESA etching up to n-GaN |
| n-Pad | | n-pad, ITO MQW + p-Gan, n-GaN, Sapphire | ✓ N-Pad deposition ✓ Aligning the height of the p - side |
| Passi open | | n-pad, ITO MQW + p-Gan, SiO₂, n-GaN, Sapphire | ✓ Overall SiO2 deposition (passivation) ✓ SiO2 etching, UBM deposition open |
| UBM | | n-pad, UBM, ITO MQW + p-Gan, SiO₂, n-GaN, Sapphire | ✓ n,p-UBM deposited at the same time ✓ Au termination |

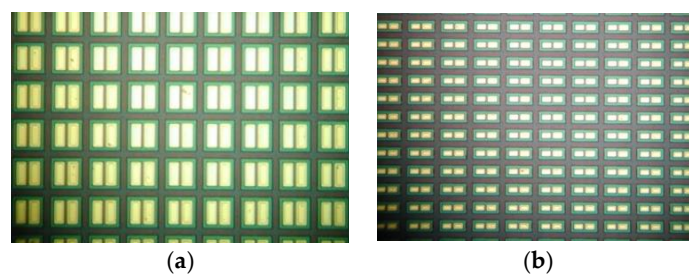**Figure 4.** Fabrication steps for the UV μLED chip.



(**a**)  (**b**)

**Figure 5.** UV micro LED chip. (**a**) Square; (**b**) Rectangle.

For the eight types of μLED chips with four different substrates and emission wavelengths, before dicing the chips as shown in Figure 6, the needles of the prober were connected with the

p electrode and the n electrode of the chip formed on the wafer such that the emission spectrum, voltage transition vs. injection current (I–V characteristics), and emission intensity vs. injection current (I–L characteristics) could be measured. The light that passed through the substrate having a thickness (140 μm) several times as large as the chip was measured using a spectrometer located at a fixed distance from the substrate; hence, relative differences in intensity caused by the differences in size could be accurately understood even though the measured value was relative intensity. In addition, the current density used in the measurements was kept constant to consider the size difference in equal terms. Furthermore, crystallinity was evaluated via X-Ray Diffraction (XRD) and Atomic Force Microscope (AFM), and the relationship with efficiency was also analyzed.
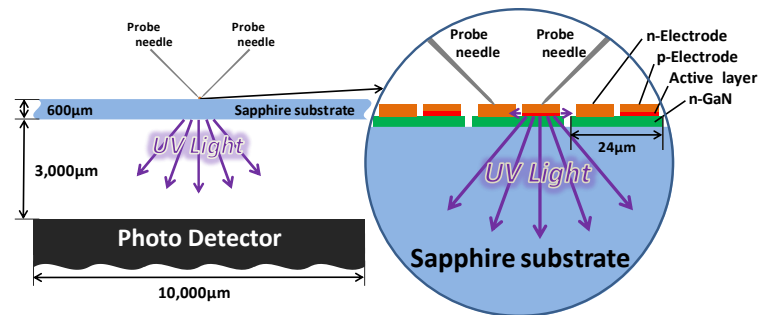


**Figure 6.** Measurement method with prober.

## 3. Results

### 3.1. Emission Spectrum

The emission spectra of μLED chips of eight different sizes that emit at 385 nm and 400 nm on a sapphire substrate and PSS were measured at a current density of 25.5 A/cm$^2$. In the emission spectra shown in Figure 7, the spectra are mostly identical for all chip sizes. In addition, the substrate had no effect on the emission waveform. However, owing to the difference in wavelength, the emission intensity differed at the deep level of GaN, i.e., around 500–550 nm. A chip emitting at 385 nm should include a wavelength band near the band gap (3.4 eV: 365 nm) of GaN; that light in the active layer excites the GaN layer and increases the light emission intensity around 500–550 nm.
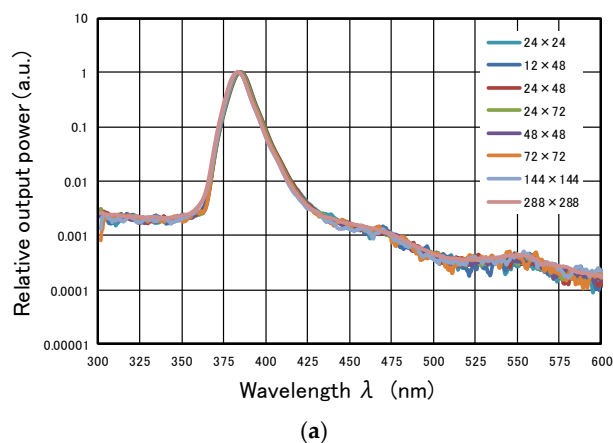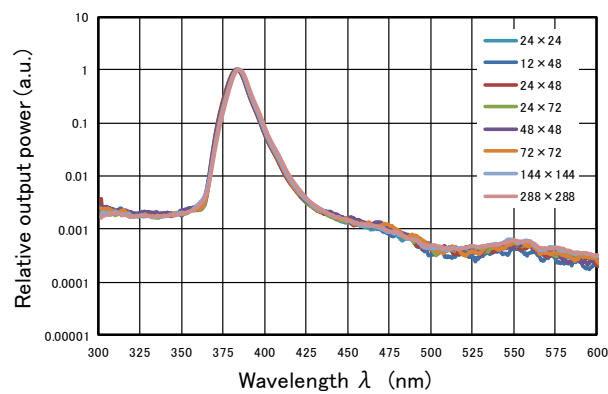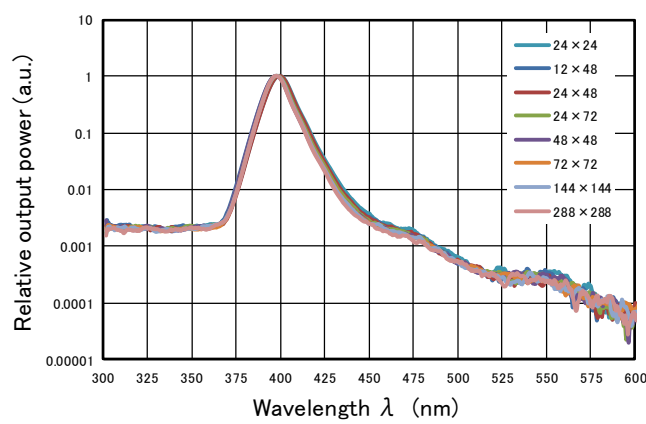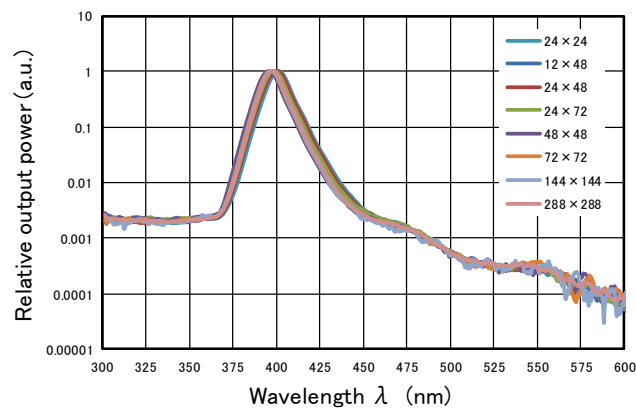


(**a**)
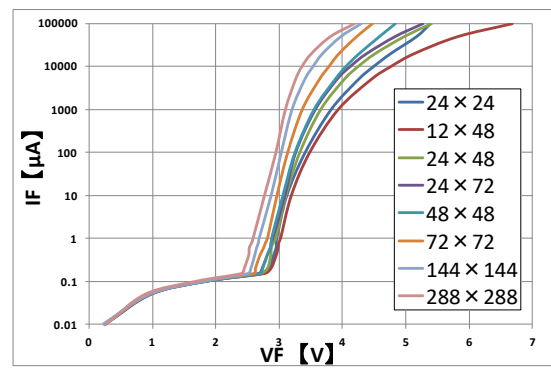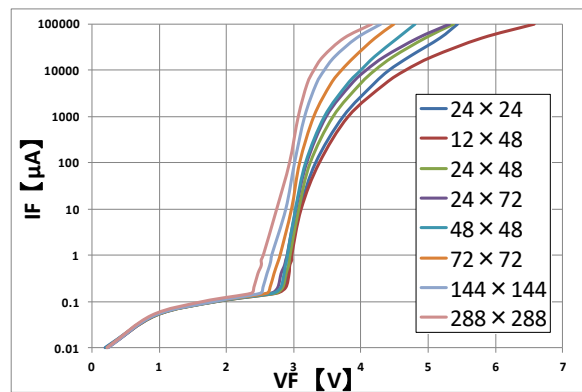
**Figure 7.** *Cont.*

(**b**)



(**c**)



(**d**)

**Figure 7.** Emission spectra. 385-nm LED: (**a**) sapphire substrate, (**b**) PSS; 400-nm LED: (**c**) sapphire substrate, (**d**) PSS.
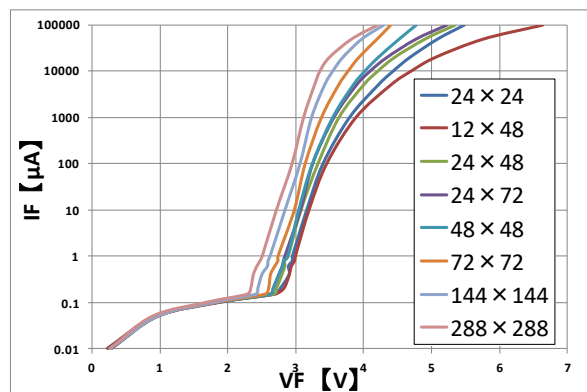
### 3.2. I–V Characteristics

Figure 8 shows the I–V characteristics of the chips, and Figure 9 shows the current density of the chips and their Forward Voltage (VF) values at 25.5 A/cm$^2$. Even as the chip size was decreased, the I–V characteristics were normal with no leakage in the low-current region. At the current density of 25.5 A/cm$^2$, VF was 3.4–3.6 V regardless of the substrate.
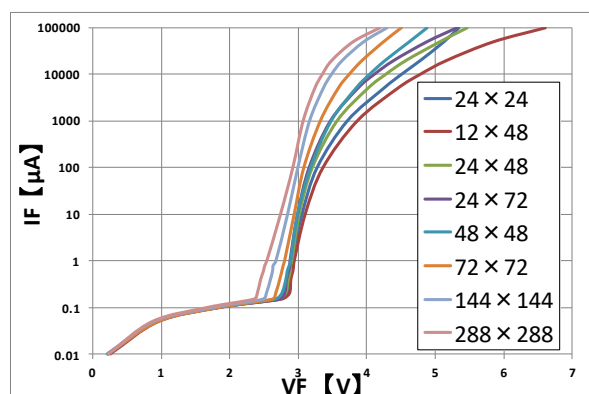
(**a**)



(**b**)



(**c**)



(**d**)

**Figure 8.** Measured I–V characteristics. 385-nm LED: (**a**) sapphire substrate (**b**) PSS; 400-nm LED: (**c**) sapphire substrate, (**d**) PSS.
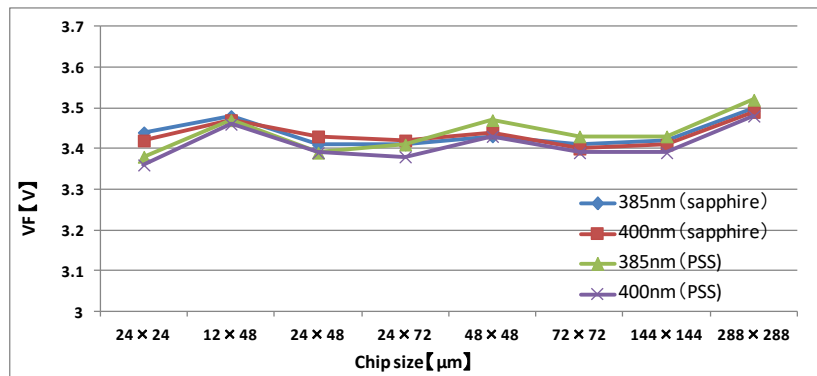
**Figure 9.** VF characteristics of chips at a current density 25.5 A/cm$^2$.

### 3.3. I–L Characteristics

Figure 10 shows the measured I–L characteristics as the current density was increased from 25.5 A/cm$^2$ to 357.1 A/cm$^2$. Despite the droop phenomenon because of which luminous efficiency decreases as the current density increases, relatively good characteristics were observed from all chips. Interestingly, as the current density increases, the EQE tended to decrease in the 400-nm chips.
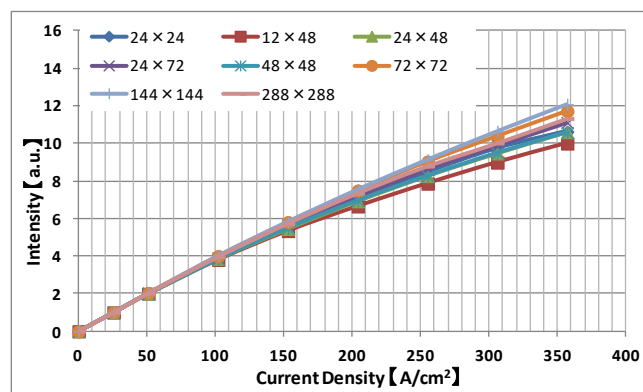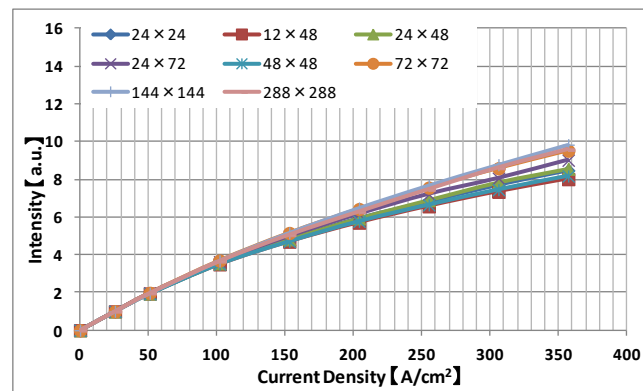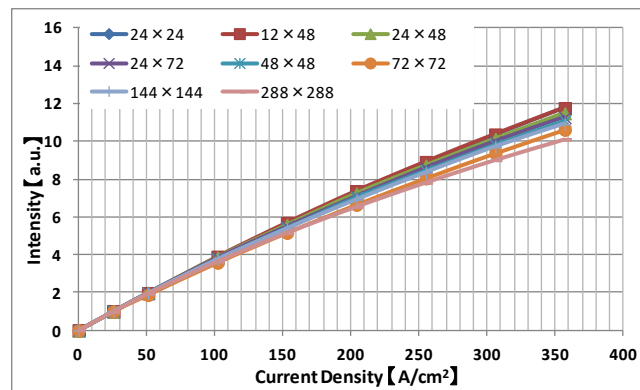


(**a**)
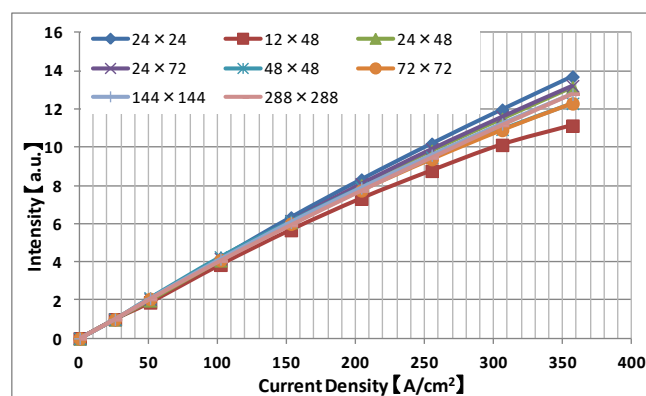


(**b**)

**Figure 10.** *Cont.*

(**c**)



(**d**)

**Figure 10.** Measured I–L characteristics. 385-nm LED: (**a**) sapphire substrate (**b**) PSS; 400-nm LED: (**c**) sapphire substrate, (**d**) PSS.

Chips fabricated on a PSS substrate displayed better I–L characteristics than those on the sapphire substrate. To verify the results, samples with the structure shown in Figure 2 were grown up to the final InGaN layer of Multi Quantum Well (MQW)s for wavelengths of 385 and 400 nm. These samples were measured for In composition and crystallinity of the light-emitting layer via XRD. Table 1 and Figure 11 show the results of the XRD measurements. The compositions of the luminescent layer (InGaN), were $In_{0.08}Ga_{0.92}N$ for 385 nm, and $In_{0.13}Ga_{0.87}N$ for 400 nm. The XRD full width at half maximum (FWHM) (0002) was narrower in the PSS-substrate chips were narrower than the sapphire-substrate chips.

**Table 1.** Measured XRD of Last-InGaN.

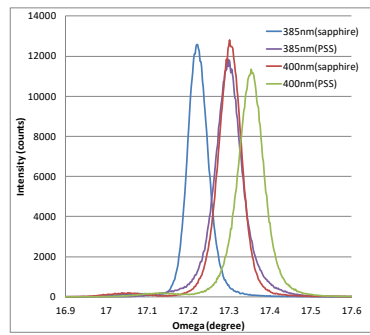|  | In Composition | InGaN XRD FWHM (arcsec) |
| --- | --- | --- |
| 385 nm (sapphire) | $In_{0.079}Ga_{0.921}N$ | 374.4 |
| 385 nm (PSS) | $In_{0.081}Ga_{0.919}N$ | 360 |
| 400 nm (sapphire) | $In_{0.134}Ga_{0.866}N$ | 388.8 |
| 400 nm (PSS) | $In_{0.134}Ga_{0.866}N$ | 360 |

**Figure 11.** XRD Spectrum of Last-InGaN.

Figure 12 shows the AFM observations of the InGaN surface (the final layer of MQW). The dislocation density in the 385-nm chip on sapphire was $2.12 \times 10^8$ cm$^{-2}$, the dislocation density in the 385-nm chip on PSS was $1.72 \times 10^8$ cm$^{-2}$, the dislocation density in the 400-nm chip on sapphire was $2.52 \times 10^8$ cm$^{-2}$, and the dislocation density in the 400-nm chip on PSS was $1.08 \times 10^8$ cm$^{-2}$.
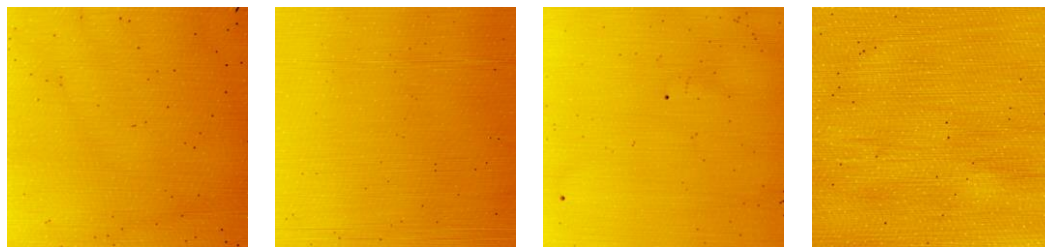


**Figure 12.** AFM images. (**a**) 385-nm (left: sapphire substrate, right: PSS); (**b**) 400-nm LED (left: sapphire substrate, right: PSS).

*3.4. Emission Intensity*

Figure 13 shows the method and measurement results of emission intensity when applying a current density of 25.5 A/cm$^2$ with the prober. Regardless of the sapphire substrate and PSS, higher emission intensities than 385 nm were obtained at 400 nm from all chip sizes.
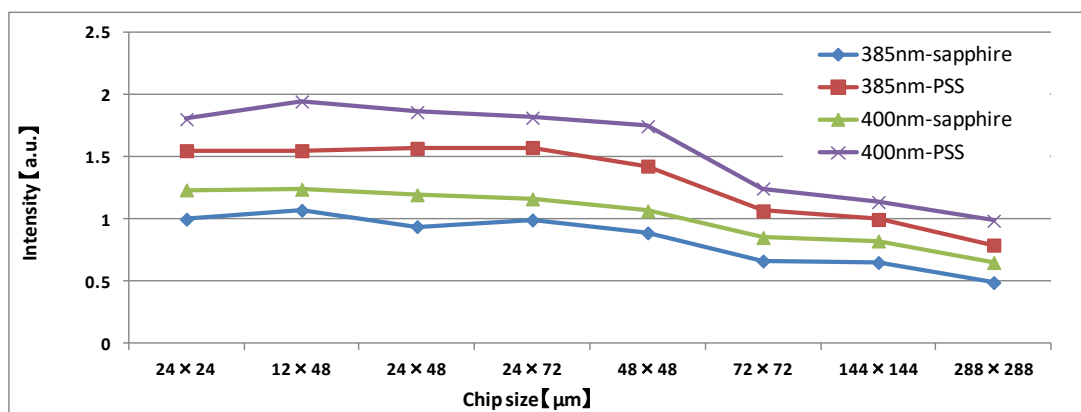


**Figure 13.** Luminescence intensity measured by prober.

In addition, when compared with the chips fabricated on the sapphire substrate, the emission intensity was found to be larger in the chips fabricated on the PSS substrate. This finding confirmed that the emission intensity increases by about 1.5 times even if the chip size is reduced, and we can ensure the luminous efficiency of a PSS-substrate chip even in a UV μLED chip that is 50 μm or smaller in size. Table 2 and Figure 14 show the XRD measurement results for 385-nm and 400-nm chips grown on the sapphire substrate and PSS.

**Table 2.** Measured XRD of n-contact layer.

|  | **(0002)** | **(10–12)** |
|---|---|---|
| 385 nm (sapphire) | 239.6 | 249.9 |
| 385 nm (PSS) | 240.9 | 223.7 |
| 400 nm (sapphire) | 226 | 244.6 |
| 400 nm (PSS) | 238.8 | 220.4 |



(**a**)                                             (**b**)
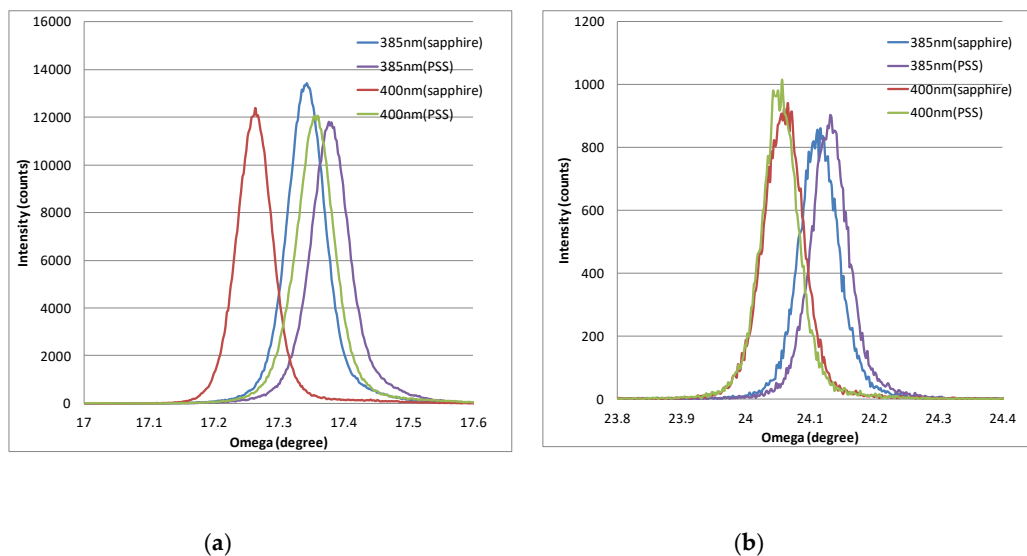
**Figure 14.** XRD Spectrum of n-contact layer. (**a**) 0002, (**b**)10–12.

## 4. Discussion

As the results of the I–L characteristics, the EQE decreased at the 400-nm chip with increasing current as compared with 385 nm. Since the density of In in the light-emitting layer (InGaN) is larger at 400-nm chip, the IQE is higher due to the effect of nonuniformity of In composition. However, the crystallinity of InGaN is poor because the content of In is large. Therefore, when the current is increased, the influence of crystal defects in the light emitting layer increases non-radiative recombination, and the IQE decreases.

The result of emission intensity shows that if the chip is fabricated at microscale, the radiative recombination rate is not affected by the nonuniformity of In composition. Interestingly, as the chip size decreases, the emission intensity tends to increase. This unexpected trend may be explained by the shorter distance of the diffusion current in smaller chips, which would improve the activity of emission recombination and improve the IQE.

Based on the results shown in Table 2 and Figure 14, the XRD FWHM is narrower in the (10–12) plane of the n-contact layer in the chip grown on the PSS, it is thought that dislocations of the n-contact layer are reduced. The light emitting layer (InGaN) grown thereon has a reduced dislocation density and improved crystallinity (Figure 12). As a result, the IQE is improved, and by extension, the luminescence intensity improves.

## 5. Conclusions and Further Work

The development of μLED displays has rejuvenated interest in IQE. Cost is a central concern for industrial applications, and the widespread adoption of LED lighting has encouraged improvement in the light extraction efficiency of InGaN-type LEDs. In contrast, for LEDs emitting in the UV region, usually used as substitutes for UV lamps, the development of a crystal structure that improves IQE has proceeded without regard for cost. As a result, the EQE of mass-produced UV-LEDs from our company,

which emit around 385 nm, exceeds 60%, which is equivalent to that of a blue LED, the efficiency of which is enhanced by the fluctuation of In composition. Red LEDs have just entered development using other materials to reduce their dimensions to the microscale, and green LEDs face an urgent need to solve the efficiency droop effect. However, these problems are easily solved with the method of RGB phosphor and UV-LEDs, so UV-μLED Display may lead others. In the future, to improve the IQE of μLEDs, researchers will need to carefully consider the material, chip size, wavelength, current, and other parameters. This study validated evidence regarding the IQE of these chips through tests of micro-sized LED chips that emit in the near-UV wavelength range. Measurements of emission spectra and I–V and I–L characteristics confirmed that desirable electrical characteristics were obtained regardless of the substrate and that the characteristics become more stable when the UV-LED is downsized to form a μLED. This work was made possible through continuous effort over many years to improve crystalline quality, unevenness in composition, and to reduce internal absorption to improve IQE.

## 6. Patents

Patent pending (Japanese Patent Application No. 2018-181017 and No. 2018-199891

**Author Contributions:** Conceptualization, Y.M., M.K. and A.K.; Investigation, M.K. and A.K.; Project administration, Y.M.; Supervision, Y.M.; Visualization, M.K. and A. K.

## References

1.	Woodgate, G.J.; Harrold, J. Micro-Optical Systems for Micro-LED Displays. *SID* **2018**, *49*, 1559–1562. [CrossRef]
2.	Lee, V.W.; Twu, N.; Kymissis, I. Micro-LED Technologies and Applications. *SID* **2016**, *32*, 16–22. [CrossRef]
3.	Chong, W.C.; Wong, K.M.; Liu, Z.J.; Lau, K.M. A Novel BLU-Free Full-Color LED Projector using LED on Silicon–Displays. *IEEE Photonics Technol. Lett.* **2013**, *25*, 2267–2270.
4.	OPTRINICS ONLINE. Available online: http://www.optronics-media.com/news/20180607/51570/ (accessed on 19 December 2018).
5.	Sato, Y.; Sato, S. Monte Carlo Simulation on Properties of a Novel Flat-Panel Fluorescent Display Excited by GaN Micro-Ultraviolet-Light-Emitting Diodes. *Jpn. J. Appl. Phys.* **2000**, *39*, 11. [CrossRef]
6.	Hwang, J.I.; Hashimoto, R.; Saito, S.; Nunoue, S. Development of InGaN-based red LED grown on (0001) polar surface. *Appl. Phys.* **2014**, *7*, 071003. [CrossRef]
7.	Zhu, W.; Mitchell, B.; Timmerman, D.; Koizumi, A.; Gregorkiewicz, T.; Fujiwara, Y. High-Power Eu-Doped GaN Red LED Based on a Multilayer Structure Grown at Lower Temperatures by Organometallic Vapor Phase Epitaxy. *MRS Adv.* **2017**, *2*, 159–164. [CrossRef]
8.	Narukawa, Y.; Ichikawa, M.; Sanga, D.; Sano, M.; Mukai, T. White light emitting diodes with super-high luminous efficacy. *J. Phys. D Appl. Phys.* **2010**, *43*, 35. [CrossRef]
9.	Stauss, P.; Walter, A.; Baur, J.; Hahn, B. 7th International Conference on Nitride Semiconductors (ICNS-7), Las Vegas, NV, USA, 16–21 September 2007. Available online: http://malcat.uum.edu.my/kip/Record/usm.269551 (accessed on 28 January 2019).
10.	Piprek, J. Efficiency droop in nitride-based light-emitting diodes. *Appl. Mater. Sci.* **2010**, *207*, 2217–2225. [CrossRef]
11.	Cho, J.; Schubert, E.F.; Kim, J.K. Efficiency droop in light-emitting diodes: Challenges andcountermeasures. *Laser Photonics Rev.* **2013**, *7*, 408–421. [CrossRef]

12. Muramoto, Y.; Kimura, M.; Dempo, A.; Nouda, S.; Fukawa, Y. Application of UV-LEDs to the LCD Backlights. Display Week 2010. In Proceedings of the 48th SID International Symposium, Seminar & Exhibition, 66.1. Washington State Convention Center, Seattle, Washington, DC, USA, 23–28 May 2010.

13. Muramoto, Y.; Kimura, M.; Dempo, A.; Nouda, S.; Fukawa, Y. Application of UV-LED to the LCD Backlight. *SID* **2010**, *41*, 982–984. [CrossRef]